

Resonance-Enhanced Excitation of Interlayer Vibrations in Atomically-Thin Black Phosphorus

Nannan Mao,^{†,⊥} § Yuxuan Lin,[†] Yaqing Bie,[¶] Tomás Palacios,[†] Pablo Jarillo-Herrero,[¶] Liangbo Liang,^{||} Xi Ling,[§] Jing Kong,^{†,} William Tisdale^{⊥,*}*

[†]Department of Electrical Engineering and Computer Sciences, Massachusetts Institute of Technology, Cambridge, Massachusetts 02139, United States

[⊥]Department of Chemical Engineering, Massachusetts Institute of Technology, Cambridge, MA 02139, United States

[§] Department of Chemistry and Division of Materials Science and Engineering, Boston University, Boston, Massachusetts 02215, United States

[¶] Department of Physics, Massachusetts Institute of Technology, Cambridge, MA 02139, United States

^{||} Center for Nanophase Materials Sciences and Computational Sciences and Engineering Division, Oak Ridge National Laboratory, Oak Ridge, Tennessee 37831, United States

KEYWORDS: rigid-layer lattice vibrations, black phosphorus, resonance Raman scattering, interlayer interaction, interband electronic transitions

ABSTRACT

The strength of interlayer coupling critically affects the physical properties of two-dimensional (2D) materials. In particular, black phosphorus (BP) – an anisotropic elemental 2D semiconductor – has been theoretically predicted to have strong interlayer interactions due to significant charge redistribution, giving rise to the well-known layer dependence of the electronic structure in few-layer BP. However, the strength of interlayer coupling in BP has not been experimentally validated. In principle, rigid-layer vibrations reflect directly the interlayer coupling strength in 2D van der Waals solids, but measurement of these characteristic frequencies is made difficult by sample instability and small Raman scattering cross-sections in atomically-thin elemental semiconductors. Here we overcome these challenges in BP by performing resonance-enhanced low-frequency Raman scattering under an argon protective environment. Interlayer breathing modes for atomically-thin BP were unobservable under conventional (non-resonant) excitation but became strongly enhanced when the excitation energy matched the subband electronic transitions of few-layer BP, down to bilayer thicknesses. Notably, the measured out-of-plane interlayer force constant was found to be 7.3 N/atom in BP, which is 2.8 times larger than graphene. These measurements directly confirm strong interlayer coupling in BP, and lay the foundation for future exploration of BP twisted structures and heterostructures.

Interlayer interaction in two-dimensional (2D) materials plays a crucial role in electronic band structure evolution of atomically-thin layered materials.^{1,2} For example, MoS₂ undergoes a transition from indirect band gap in bulk and few-layer to direct band gap in monolayer, leading to significant excitonic character of the band edge absorption and emission spectra.³ Moreover,

2D layers stacking together via van der Waals interaction with twisted angles has shown fascinating physical phenomena, such as superconductivity in magic angle graphene.⁴ Van der Waals interactions can also hold different combinations of 2D layers together, forming van der Waals heterostructures⁵ that provide an exciting platform for the manipulation of interlayer excitons, electron-phonon, and electron-photon interactions.^{6,7} Consequently, the strength of interlayer coupling is one of the key parameters that profoundly governs the physical properties of 2D materials and their heterostructured building blocks.

Black phosphorus (BP) is an emerging elemental 2D semiconductor, which has a puckered structure formed by sp^3 hybridized P atoms.⁸⁻¹⁰ Due to the interlayer interaction, the valence band and conduction band in few-layer BP split into multiple subbands, giving rise to thickness-dependent direct band gap and a series of optical resonances (called subband electronic transitions) between the van Hove singularities in the visible and infrared regime. Its band gap is tunable from 0.34 eV in the bulk to 1.73 eV in the atomically-thin limit.^{2,11} Given such sensitive dependence of electronic structure on layer number, theoretical studies have explored the nature of interlayer interactions in BP, finding that these interactions arise in part from significant interlayer charge redistribution rather than pure van der Waals character.¹² Furthermore, the adhesion energy and the exfoliation energy in BP were predicted to be significantly larger than other 2D materials such as graphene and transition metal dichalcogenides (TMDs).^{9,12-15} Despite the importance of this fundamental parameter, the direct measurement of the interlayer coupling strength in BP is lacking.

Collective interlayer vibrations in 2D materials, which usually occur at low frequency ($<100\text{ cm}^{-1}$), reflect directly the interlayer interaction between neighboring layers. For BP, previous works have attempted to measure these collective interlayer oscillations under ambient conditions.¹⁶⁻¹⁸

However, due to the ambient instability of few-layer BP samples, the interlayer vibrational modes in atomically-thin BP – especially down to bilayer thickness – has not been observed.¹⁶⁻¹⁸ Moreover, the scattering probability of the interlayer acoustic modes in few-layer elemental 2D materials is extremely low,¹⁹⁻²¹ which raises another challenge for their observation in atomically-thin BP. Given these challenges, the quantitative determination of the interlayer coupling strength in BP has remained a theoretical endeavor.¹⁶⁻¹⁸

Here we overcome the challenges of low-frequency Raman scattering in atomically-thin BP by using resonance-enhanced Raman scattering under an argon-protective atmosphere. The interlayer vibration modes in atomically-thin BP were unobservable at conventional excitation wavelengths, but turned on when the excitation energy matched an interband electronic transition above the band gap. Our results demonstrate that resonance effects are a critical consideration for observing the full series of thickness-dependent interlayer vibrations in 2L-11L BP. These modes shift in frequency from 63.3 cm^{-1} for bilayer to 11.8 cm^{-1} for 11L. Notably, the estimated out-of-plane interlayer force constant is 7.3 N/atom in BP, which is 2.8 times larger than that of graphene (2.6 N/atom ^{18,20}), confirming the significantly stronger interlayer interaction in BP. This work offers fundamental insights into the interlayer interaction in BP, which will facilitate the understanding and future exploration of BP related twisted structure and heterostructure.

Results and Discussion

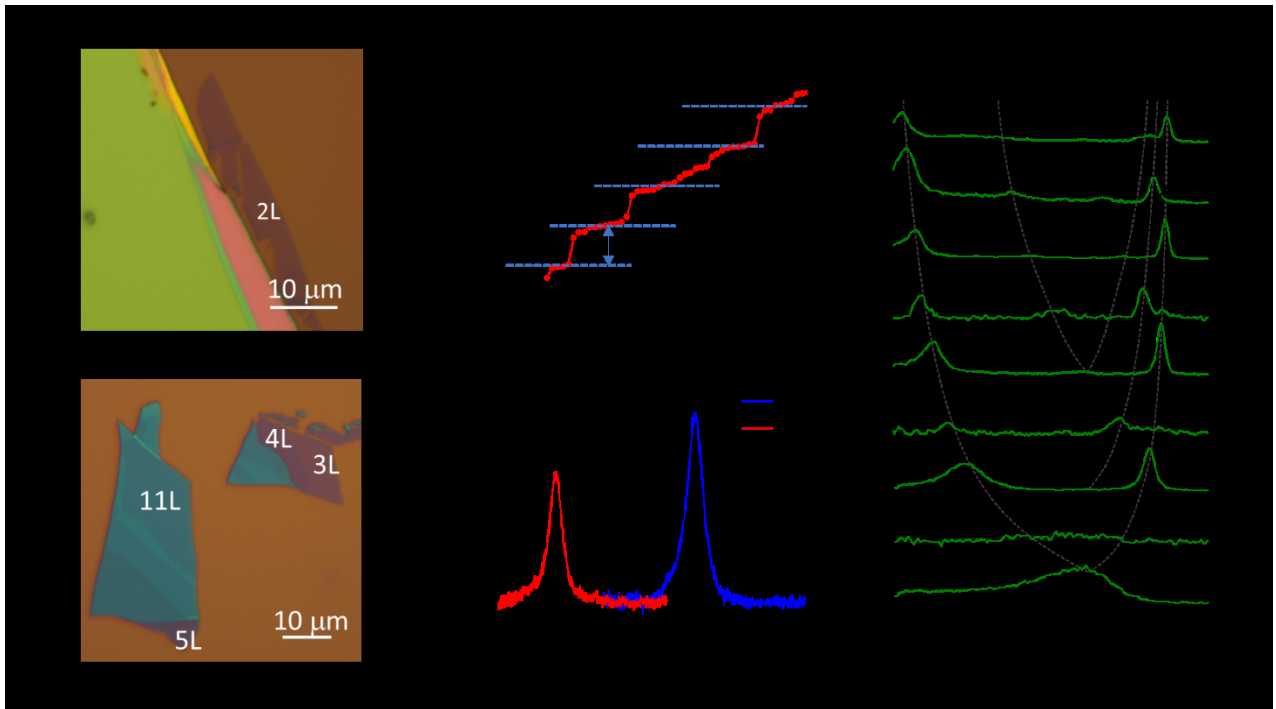


Figure 1. Characterization of few-layer phosphorus samples. (a, b) Optical images of few-layer BP samples marked with layer numbers. (c) Optical contrast (red channel) measured on 50 different few-layer BP samples; each data point here corresponds to one sample. (d) Photoluminescence spectra of 2L (blue line) and 3L (red line) BP samples excited at 635 nm. (e) Thickness-dependent low-frequency Raman spectra of 2L-10L BP at the excitation energy of 2.33 eV. The Raman intensity of 3L, 5L and 7L was scaled by 5 times and 9L by 2.5 times to illustrate high-order low frequency Raman branches. The grey dash lines are guides for the eye.

Sample preparation and thickness determination. Few-layer BP samples were mechanically exfoliated onto a 285 nm SiO₂/Si substrate in an argon-gas glove box. Since atomically-thin BP flakes are unstable in air, their thicknesses were determined by optical images (Figure 1a and 1b) and photoluminescence (PL) spectra measured under inert argon atmosphere. To establish an accurate method to determine their thicknesses, we analyzed optical contrasts of more than 50 few-layer BP samples by extracting the pixel intensity value of the red channel from full-color

optical images. The optical contrast was determined by dividing the on-flake intensity value by the off-flake (i.e. bare substrate) intensity value. As shown in Figure 1c, optical contrasts of these samples display a step-like increase with the thickness. The averaged step increase, which represents that the contrast difference between two adjacent thickness, was approximately 0.08. Furthermore, the averaged optical contrast of the thinnest sample in Figure 1c is close to the step contrast, suggesting that the thinnest samples here are monolayers. Since optical contrasts of layered materials show linear dependence on their thickness for very thin flakes,²² this method allowed us to distinguish the thickness of few-layer BP samples as annotated in Figure 1a and 1b. To further confirm the thickness, we measured the PL spectra of these samples (Figure 1d) with 635 nm laser. 2L and 3L BP show PL peaks at 1.13 eV (1095 nm) and 0.86 eV (1438 nm), respectively, which are consistent with previous reports.² Excitonic emission from monolayer and other thickness beyond 3L are out of the efficient detection range of the InGaAs detector (800 nm-1.7 μ m) used. To determine the thicknesses of BP flakes thicker than 9L, we used the brightness of the optical image measured through the green channel (Figure S1) and the low-frequency Raman spectrum for additional validation.

Thickness-dependent low-frequency Raman spectra. Figure 1e shows low-frequency Raman spectra in 2L-10L BP excited at 2.33 eV, which were measured under parallel polarization with both the incident and collection polarizations along armchair (AC) direction of BP. Spectra were measured on a micro-Raman spectrometer in backscattering geometry (see Experimental Section). The crystalline orientations of these samples were identified by angle-dependent polarized Raman intensities of high-frequency Raman modes^{10,23-25}. Notably, we were able to observe one broad low-frequency Raman peak at 63.3 cm^{-1} in 2L BP, which has not previously been reported; the observation of this low-frequency Raman mode in the bilayer sample is

essential for accurate determination of interlayer interactions. This low-frequency Raman peak redshifted as the thickness increased from a value of 63.3 cm^{-1} in 2L BP to 12.7 cm^{-1} in 10 L BP. Moreover, we note that the Raman intensities in odd-layer samples were consistently weaker than in even-layer samples, as shown in Figure 1e. In 3L BP, no low-frequency Raman peaks were observed at all with the excitation energy of 2.33 eV.

According to theoretical analysis^{16,17}, for NL BP (where N is the number of layers in thickness), there are $2(N-1)$ in-plane shear modes and $N-1$ out-of-plane breathing modes. The shear modes correspond to horizontal displacement of the rigid layers, whereas the breathing mode corresponds to vertical displacement of atoms on neighboring layers. Given that BP is an anisotropic crystal, half of the shear modes are polarized along AC direction while the other half are polarized along zigzag (ZZ) direction. They are either Raman active (B_{3g} or B_{1g}) or infrared active (B_{1u} or B_{3u}) in an alternating sequence with its frequency. Similarly, the $N-1$ interlayer breathing mode can be either Raman active (A_g) or infrared active (B_{2u}). However, because of the symmetry of the Raman tensor and the incident and collection geometry, B_{3g} and B_{1g} modes are not allowed in backscattering configuration and could not be observed in our experiment.^{17,18,26} Therefore, we conclude that the Raman modes observed in Figure 1e correspond to the interlayer breathing modes in BP with A_g symmetry. These modes are labeled $B_{N,n}$, indicating the n^{th} ($n=1, 2, 3, \dots, N-1$) breathing mode in N layer BP, whose frequency decrease with sequence number n. For example, $B_{N,1}$ corresponds to the highest frequency branch, while $B_{N,N-1}$ the lowest frequency branch in N layer BP. As shown in Figure 1e and S2, we could observe five low-frequency Raman branches: $B_{N,1}$ $B_{N,2}$ $B_{N,3}$ $B_{N,N-3}$ and $B_{N,N-1}$. Three of them show a smooth blueshift while two of them show a redshift trend with increasing of the layer number N. In addition, the total number of low-frequency modes observed in NL BP are

always equal to or smaller than $(N-1)/2$ (N is odd number) or $N/2$ (N is even number). Moreover, the lowest frequency branch $B_{N, N-1}$ which represents the softest mode (with surface layer out-of-phase)¹⁷ are always observed for all thicknesses except for 3L at excitation of 2.33 eV. In contrast, the highest frequency branch $B_{N, 1}$ are mostly allowed for even-layer BP and second-highest frequency branch $B_{N, 2}$ are Raman-active for odd-layer BP. These trends are consistent with group theory analysis and first-principles calculations for interlayer breathing modes of BP in prior works,^{17,18} and also similar to other 2D materials such as MoTe₂ and MoS₂,^{27,28} which further confirms that all branches observed in Figure 1e belong to interlayer breathing modes.¹⁴

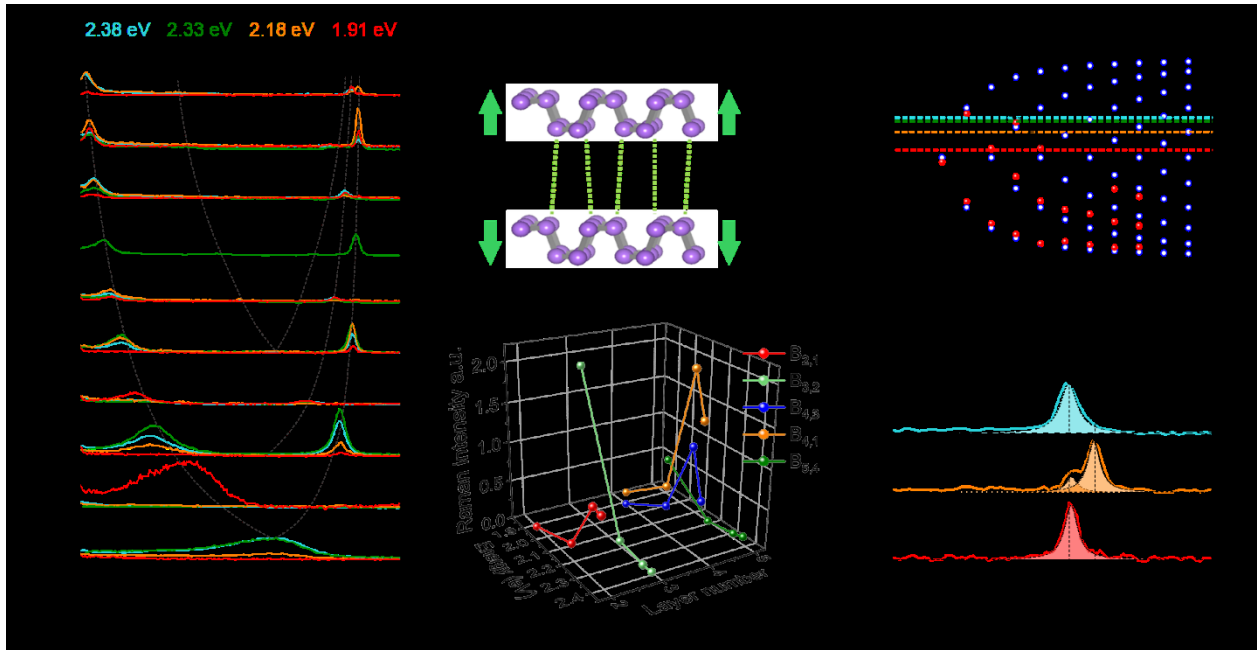


Figure 2. Resonance excitation of interlayer vibrations in few-layer BP. (a) Normalized thickness-dependent low-frequency Raman spectra of 2L-11L BP excited at 2.38 (blue), 2.33 (green), 2.18 (orange) and 1.91 eV (red). Different color spectra correspond to the different excitation energies, as indicated at the top of the figure. The grey dash lines are guides for the eye to highlight the frequency shift of interlayer vibration modes. (b) Displacement pattern of the

collective interlayer breathing mode in bilayer BP. (c) Four Raman excitation energies (dashed lines) with respect to the calculated (blue opened circle) and measured (red dots) subband transition energies in few-layer BP from previous reports.^{2,29,30} (d) Excitation-energy-dependent Raman intensities of the interlayer vibration modes in 2L-5L BP. (e) Normalized Raman spectra of 11L BP excited at 2.38, 2.18 and 1.91 eV. The black dash lines are guides for the eye to highlight the same interlayer vibration modes.

Electronic resonance effect on rigid-layer interlayer vibrations in few-layer BP. Figure 2a displays the thickness-dependent low-frequency Raman spectra in 2L-11L BP excited at 2.38, 2.33, 2.18 and 1.91 eV, with both the incident and collection polarizations along AC direction. All of the Raman spectra in Figure 2a were normalized to the Raman intensity of a reference single crystalline quartz peak at 465 cm^{-1} . From the normalized Raman spectra under multiple excitation energies, we could observe low-frequency Raman peaks for each thickness. The broad low-frequency Raman peak at 63.3 cm^{-1} ($B_{2,1}$) in 2L BP was observed at excitation energies of 2.38 and 2.33 eV. As discussed in the preceding section, this mode corresponds to the interlayer breathing mode as illustrated in Figure 2b. In 3L BP – where no low-frequency Raman feature was observed at 2.33 eV – a significant peak at 39.0 cm^{-1} could be observed with the excitation energy tuned to 1.91 eV. These two modes belong to the lowest frequency branch, which shows a large redshift with increasing number of layers as illustrated by the dashed line in Figure 2a. The frequency difference of 2L and 3L BP is 24.3 cm^{-1} , which is at same level as the case for graphene (24 cm^{-1}) while quite large compared to the case of transition metal dichalcogenides such as MoS₂ (12 cm^{-1})²⁷ and MoTe₂ (9 cm^{-1})²⁸.

The excitation energy dependence of the low-frequency Raman spectra in few-layer BP, as shown in Figure 2a, is a striking consequence of electronic resonance. Taking 2L and 3L BP

samples as examples, it can be seen that the breathing mode $B_{2,1}$ in 2L is hardly noticeable at excitation energy of 1.91 eV, which shows slightly stronger intensity at 2.18 eV. Surprisingly, it turns into a very broad and salient peak at 63.3 cm^{-1} when excited at 2.33 and 2.38 eV. In contrast, for 3L BP, a significant low-frequency Raman peak at 39.0 cm^{-1} appears at excitation of 1.91 eV while is absent at other excitation energies. This phenomenon can be attributed to the intrinsic resonance effect with subband electronic transitions above the band gap. Due to quantum confinement in the out-of-plane direction, NL BP shows similar electronic structure as traditional quantum wells, which vary significantly with thicknesses.^{2,29,30} The conduction band and valence band split into N quantized subbands $E_{N,n}$ at the Γ point of Brillouin zone (Figure S3) in the visible and near infrared region, where $E_{N,n}$ represents the n^{th} ($n=1, 2, 3, \dots, N-1$) subband electronic transitions in NL BP (Figure 2c).^{2,29,30} Consequently, when the excitation energy matches with one of the higher subband electronic transitions, Raman intensity of the corresponding breathing modes will be dramatically enhanced. For instance, as illustrated in Figure 2c, excitation lasers with energies of 2.38 (520 nm) and 2.33 eV (532 nm, green line) are in near resonance with the second subband electronic transition $E_{2,2}$ (2.44 eV) in 2L BP, which has been previously confirmed by the optical reflection measurement.² This explains why the low-frequency Raman peak at 63.3 cm^{-1} was not observed in 2L BP in previous investigations where the excitation wavelength was limited to 633 nm (1.96 eV),¹⁶⁻¹⁸ which is out of the resonance window. On the other hand, 1.91 eV (648 nm) excitation is closely resonant with $E_{3,3}$ (1.93 eV, Figure 2c) in 3L BP, leading to strong low-frequency Raman peak at 39.0 cm^{-1} . These observations reinforce the importance of resonance effects for accurate determination of breathing modes in few-layer BP.

To further explore the resonance effect on breathing modes in few-layer BP, we plotted the excitation-energy dependent low-frequency Raman intensities in 2L-5L. As shown in Figure 2d, the resonance energy of interlayer breathing modes varies with thickness, reflecting the thickness-dependent electronic structure of BP. For 4L BP, Raman resonance for both mode $B_{4,1}$ and $B_{4,3}$ occurs at 2.33 eV, close to the energy of the third subband electronic transition $E_{4,3}$ (2.31 eV, Figure 2c). 5L BP indeed shows the strongest Raman intensity at 1.91 eV, which matches the energy of the third subband electronic transition $E_{5,3}$ (1.94 eV, Figure 2c). However, as the layer number further increases (the electronic bandgap continues to decrease), only high order subbands ($E_{N,n}$, $n>3$, Figure 2c) are located in the energy range of Raman excitation lines. These bands are spanned in around one hundred of meV with smaller oscillation amplitudes, as evidenced by the weak and broad absorption peak, [2,29,30](#) which almost merge into continuous absorption background of quasi-continuous bands. Consequently, the resonance enhancement of these subband electronic transitions in thicker samples ($N>7$) are relatively weak, and interference enhancement effects might become another dominant factor. As shown in Figure S4, the calculated interference enhancement curve as a function of the excitation energy displays a peak at 2.10 eV for 9L-11L BP, which is close to the excitation energy of 2.18 eV. Therefore, in general, thicker few-layer BP samples (9L-11L) usually show slightly stronger intensity at 2.18 eV. More details about the thickness-dependent Raman intensities can be found in Table S1.

In addition to enhancement of the Raman active modes, resonance effects also contribute to the emergence of infrared-active modes in the Raman spectra. According to the theoretical results,^{[26](#)} $B_{N,1}$ mode in odd-layer BP has B_{2u} symmetry, which is infrared-active rather than Raman-active mode. Under non-resonant conditions, for instance when the excitation energies are at 2.38 and 1.91 eV, this mode was not observed in the Raman spectra of 11L BP. However, when excited at

2.18 eV – which is resonant with $E_{II,7}$ (Figure 2c) – a bright peak at 88.1 cm^{-1} ($B_{11,1}$) appears in the Raman spectra, as shown in Figure 2e. The relative intensity of $B_{11,2}$ and $B_{11,1}$ also varies obviously with the excitation energies, suggesting excitation-energy dependent electron-phonon coupling of the same Raman mode.

There is a systematic variation in the overall Raman intensity depending on whether the sample has an odd number or an even number of layers. According to the interlayer bond polarizability model,^{31,32} the $B_{N,1}$ mode scatters more strongly than $B_{N,2}$. By symmetry, only even layers exhibit the $B_{N,1}$ mode and only odd layers exhibit the $B_{N,2}$ mode. Consequently, the odd-even intensity variation may simply arise from the underlying strength of their allowed Raman transitions. However, more theoretical work is needed for full understanding.

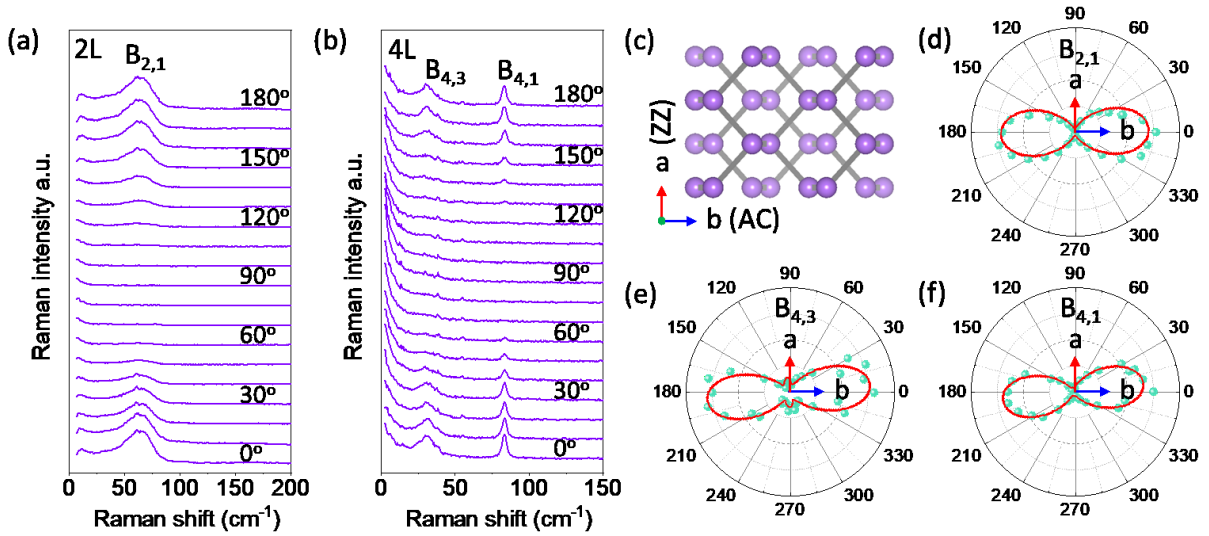


Figure 3. Symmetry assignment of collective interlayer vibrations in BP. (a, b) Polarization-dependent low-frequency Raman spectra of 2L and 4L BP excited at 2.33 and 2.18 eV, respectively. (c) The top view of atomic structure of monolayer BP with a and b indicating

zigzag (ZZ) and armchair (AC) crystalline orientations, respectively. (d-f) Polar plots of polarization-dependent Raman intensities of the collective breathing modes $B_{2,1}$ (d) in 2L, $B_{4,3}$ (e) and $B_{4,1}$ (f) in 4L BP.

Symmetry assignment of the interlayer vibrations in BP. The assignment of the low-frequency modes in BP is vital to specify the type of interlayer interaction: in-plane shear or out-of-plane compression. Even though the thickness-dependent frequency trend in our experiment has shown great consistency with theoretical predictions of the interlayer breathing modes with A_g symmetry,^{14,17} further verification of the symmetry assignment can be obtained *via* Raman selection rules. Therefore, we measured the polarization-dependent low-frequency Raman spectra of 2L and 4L BP. As shown in Figure 3a and 3b, Raman spectra of both 2L and 4L vary significantly with the sample rotation angle under parallel polarization. All of the low-frequency Raman peaks show the largest intensity when the laser polarization is along AC (0°) while almost disappear along ZZ direction (90°). The two crystalline orientations of BP are illustrated in Figure 3c. The intensity polar plots of $B_{2,1}$, $B_{4,3}$ and $B_{4,1}$ exhibit similar polarization-dependence as A_g modes in high frequency region, suggesting that all of them are indeed interlayer breathing modes of A_g symmetry.^{17,23-25,33-37}

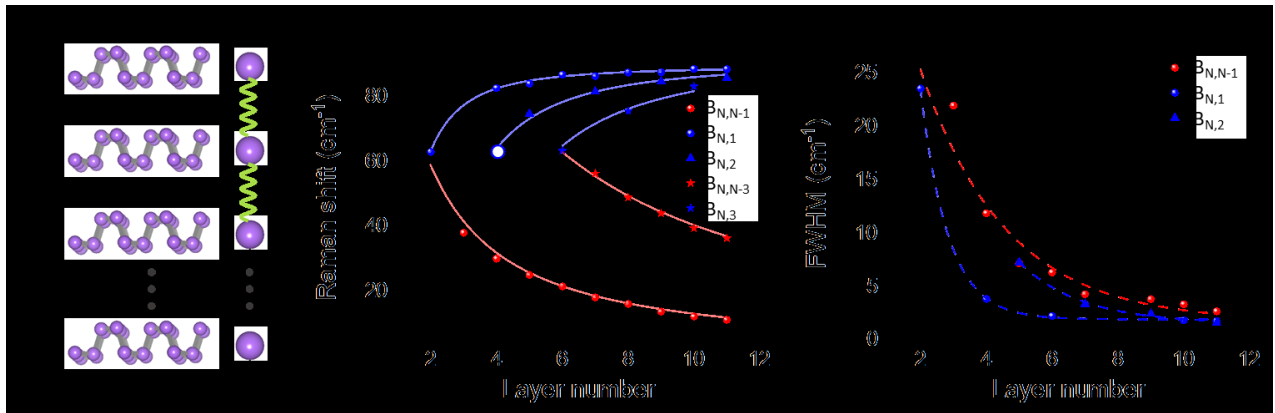


Figure 4. Frequency evolution of the interlayer breathing mode as explained by the linear chain model. (a) Schematic illustration of the linear chain model applied to BP. (b,c) Frequency evolution (b) and full width at half maximum (FWHM) of the measured interlayer breathing mode as a function of thickness. Dashed lines are guides to the eye.

Estimation of interlayer interaction in BP by linear chain model. The layer-number dependent frequency of the interlayer breathing modes can be well described by the linear chain model,^{21,32} which treats each layer as a rigid “ball” connected to its neighboring layers by a classical spring. Considering only nearest-neighbor interactions (Figure 4a), this model gives rise to N-dependent frequencies

$$\omega(B_{N,N-j}) = \sqrt{2} \omega(B_{2,1}) \sin\left(\frac{j\pi}{2N}\right) \quad (1)$$

where $\omega(B_{2,1})$ is the frequency of the breathing mode in 2L BP, and $j=1, 2, \dots, N-1$ is the branch index. In Figure 4b, we plot measured frequencies (symbols) along with best-fit lines to each branch using Equation 1. The lowest frequency branch ($B_{N,N-1}$) redshift from 63.3 cm^{-1} in 2L to 11.8 cm^{-1} for 11 L BP, which matches well with the coherent phonon modes observed by transient absorption.³⁸ Moreover, all of the branches can be fitted well by the linear chain model. In addition, based on our measured breathing mode frequency of $\omega(B_{2,1}) = 63.3 \text{ cm}^{-1}$ in 2L BP and the relation from the linear chain model $\omega(B_{bulk}) = \sqrt{2} \omega(B_{2,1})$, we can derive $\omega(B_{bulk}) = 89.5 \text{ cm}^{-1}$ for bulk BP, consistent with the experimental value of $\sim 87 \text{ cm}^{-1}$ from previous inelastic neutron scattering measurements.^{39,40}

The full width at half maximum (FWHM) of the interlayer breathing modes broadens as the thickness decreases (Figure 4c). This trend may arise from easier dissipation of phonon energy

into the surrounding environment for thinner flakes. As listed in Table S2, the fitted $\omega(B_{2,1})$ values are very close to the measured frequency of breathing mode in 2L BP, confirming that all the branches are indeed interlayer breathing modes in BP.

We note that our mode assignment disagrees with previously published work.¹⁶⁻¹⁸ Whereas all of our data are consistent with the predictions of the linear chain model, previously reported data contradicted this model, leading to speculation that unconventional behavior might be present.¹⁶⁻¹⁸ However, we attribute the inconsistency with the linear chain model in previous work to 1) mis-identification of the layer thickness, and 2) missing peaks in the series due to lack of resonance enhancement.¹⁶⁻¹⁸ Here we clarify that all the observed branches represent the in-phase or out-of-phase compression vibration of BP layers relative to neighboring BP layers in the out-of-plane direction.

The strength of the out-of-plane interaction in bilayer BP can be estimated by

$$\omega(B_{2,1}) = 1/(\sqrt{2} \pi c) \sqrt{\alpha/\mu} \quad (2)$$

where c is the speed of light and $\mu = 1.42 \times 10^{-26} \text{kg} \cdot \text{\AA}^{-2}$ is the mass per unit cell area in BP. This gives rise to the first experimental measurement of the out-of-plane interlayer force constant in BP, $\alpha = 10.1 \times 10^{19} \text{N/m}^3$. This value was predicted to be much larger than graphene and MoS₂,¹⁶⁻¹⁸ but turns out to be comparable with typical 2D vdW materials (α is $10.2 \times 10^{19} \text{N/m}^3$ and $8.9 \times 10^{19} \text{N/m}^3$ for graphene^{19,41} and MoS₂²⁷, respectively). However, BP has a highly corrugated structure, where only half of the atoms per unit area are involved in nearest-neighbor interactions, which makes it fairer to compare to more planar 2D materials like graphene on a per-atom basis. The renormalized out-of-plane constant is 7.3 N/atom in BP, which is 2.8 times

stronger than in graphene (2.6 N/atom). Our results demonstrated directly that the interlayer interaction is significantly larger in BP than graphene.

In summary, we measured the interlayer coupling strength of BP using resonance low-frequency Raman spectra under argon gas environment, which is 7.3 N /atom and 2.8 times larger than that of graphene. Our results provide direct evidence for a significantly large interlayer interaction in BP, providing insight into the nature of interlayer coupling in this material. The successful measurement of the interlayer interaction of BP was made possible by careful calibration of the layer thickness and resonance enhancement of the Raman intensity through variation of the excitation laser energy *via* interband electronic transitions in few-layer BP. The interlayer vibrational modes in atomically-thin elemental 2D materials, which are generally too weak to be observed especially in 2L-3L BP, shows significantly strong Raman intensity under resonance excitation. All of the interlayer vibration modes observed in our experiment are confirmed to be interlayer breathing modes in few-layer BP, which show thickness-dependent frequency and resonance effects in agreement with the linear chain model. The accurate identification of these frequencies also provides a quick and reliable way to determine the thickness of few-layer BP samples. The unprecedented strong interlayer coupling of BP offers the promising possibility to design and construct new optoelectronic devices based on twisted structure and heterostructure related to BP.

Experimental Section

Sample preparation and thickness characterization. Few-layer BP samples were exfoliated from bulk BP (HQ Graphene, >99.995 %) onto 285 nm SiO₂/Si substrate. The mechanical exfoliation was conducted in an argon-gas glove box (O₂ <0.1 ppm, H₂O <0.1 ppm). Optical images were

taken on an optical microscope (Nikon) inside the same glove box. Few-layer black phosphorus samples were sealed in a vacuum jar filled with argon gas before being transferred to separate microscopes for photoluminescence and Raman characterization outside the glovebox.

Infrared photoluminescence measurements. Photoluminescence of 2L-3L BP samples were measured on a micro-infrared photoluminescence spectrometer with 1D InGaAs detector array and a thermoelectric-cooled InGaAs 2D camera (Andor, iDus-InGaAs-1.7). The wavelength of the excitation laser is 635 nm (Diode laser, Thorlabs) and laser power was kept at 40 μ W. Intrinsic Si wafer (resistivity >10,000 ohm·cm) with 285 nm thickness of oxidation layer was used as substrate to avoid photoluminescence of doped silicon. A 300 gr/mm grating and a 60X objective lens (Olympus, NA=0.7) with correction ring were used to disperse and collect photoluminescence signals.

Low-frequency Raman measurements. Polarized low-frequency Raman spectra were measured on a triple-grating micro-Raman system (Horiba JY T64000) with a liquid-nitrogen-cooled charge couple detector (CCD). Four different laser lines were used in Raman measurements, 520, 568 and 648 nm from Kr⁺-Ar⁺ laser (Coherent Innova 70C) and 532 nm from solid laser (CNI, MSL-FN-532). The excitation laser beam was focused by a 60x objective lens (Olympus, NA=0.7, with correction ring) onto the sample, which was sealed in a vacuum container filled with argon gas. A BraggGrate bandpass filter and a visible grating were used to clean the plasma lines of the excitation laser. The excitation lasers are horizontally polarized and BP samples were rotated to measure the crystalline orientation-dependent polarized Raman spectra. The Raman signals are dispersed by an 1800 gr/mm grating. The laser power was kept at 0.25 mW for 520, 532 and 568 nm lasers, and 0.50 mW for 648 nm laser.

ASSOCIATED CONTENT

Supporting Information.

Green channel brightness of 7L, 9L-11L black phosphorus (BP) samples; zoomed in high order low-frequency branches, schematic illustration of the resonance Raman process in bilayer BP where the excitation energy is resonant with the second subband electronic transitions ($E_{2,2}$), interference effect in 9L-11L BP on 285 nm/SiO₂/Si substrate, thickness-dependent Raman intensities of interlayer breathing modes in few-layer BP, fitted frequency ω (B_{2,1}) for interlayer breathing mode in 2L BP based on five low-frequency branches using linear chain model.

AUTHOR INFORMATION

Corresponding Author

* jingkong@mit.edu; tisdale@mit.edu.

Present Addresses

†If an author's address is different than the one given in the affiliation line, this information may be included here.

Author Contributions

N.M., J. K., W.A.T., X.L. and L.L. initiated the project and designed the experiments. N.M. and Y.B. prepared samples. N.M. and Y.L. performed the experimental measurements. N.M., J. K., W.A.T., X.L. and L.L. analyzed the data. All authors contributed to the writing of the paper.

Notes

The authors declare no competing financial interest.

ACKNOWLEDGMENT

This work is primarily supported by U.S. Department of Energy (DOE), Office of Science, Basic Energy Sciences (BES) under Award DE-SC0020042. J.K. and N.M. also acknowledge the partial support by the Air Force Office of Scientific Research under the MURI-FATE program, Grant No. FA9550-15-1-0514. W.T. acknowledges support from the Camille & Henry Dreyfus Foundation. Y.L., T.P., and J.K. also acknowledge the partial support by the U. S. Army Research Office through the Institute for Soldier Nanotechnologies at MIT, under cooperative agreement number W911NF-18-2-0048. X.L. acknowledges the support of National Science Foundation (NSF) under Grant No. (1945364). L.L. acknowledges work conducted at the Center for Nanophase Materials Sciences, which is a US Department of Energy Office of Science User Facility. The authors thank Q. M. from MIT for the helpful suggestions on the protection of few-layer BP samples using vacuum jar.

REFERENCES

- (1) Novoselov, K. S.; Geim, A. K.; Morozov, S. V.; Jiang, D.; Zhang, Y.; Dubonos, S. V.; Grigorieva, I. V.; Firsov, A. A. Electric Field Effect in Atomically Thin Carbon Films. *Science* **2004**, *306*, 666-669.
- (2) Li, L.; Kim, J.; Jin, C.; Ye, G. J.; Qiu, D. Y.; da Jornada, F. H.; Shi, Z.; Chen, L.; Zhang, Z.; Yang, F.; Watanabe, K.; Taniguchi, T.; Ren, W.; Louie, S. G.; Chen, X. H.; Zhang, Y.; Wang, F. Direct Observation of the Layer-Dependent Electronic Structure in Phosphorene. *Nat. Nanotechnol.* **2017**, *12*, 21-25.
- (3) Splendiani, A.; Sun, L.; Zhang, Y.; Li, T.; Kim, J.; Chim, C.-Y.; Galli, G.; Wang, F. Emerging Photoluminescence in Monolayer Mos₂. *Nano Lett.* **2010**, *10*, 1271-1275.

- (4) Cao, Y.; Fatemi, V.; Fang, S.; Watanabe, K.; Taniguchi, T.; Kaxiras, E.; Jarillo-Herrero, P. Unconventional Superconductivity in Magic-Angle Graphene Superlattices. *Nature* **2018**, *556*, 43-50.
- (5) Geim, A. K.; Grigorieva, I. V. Van Der Waals Heterostructures. *Nature* **2013**, *499*, 419-425.
- (6) Eliel, G. S. N.; Moutinho, M. V. O.; Gadelha, A. C.; Righi, A.; Campos, L. C.; Ribeiro, H. B.; Chiu, P.-W.; Watanabe, K.; Taniguchi, T.; Puech, P.; Paillet, M.; Michel, T.; Venezuela, P.; Pimenta, M. A. Intralayer and Interlayer Electron–Phonon Interactions in Twisted Graphene Heterostructures. *Nat. Commun.* **2018**, *9*, 1221.
- (7) Rivera, P.; Schaibley, J. R.; Jones, A. M.; Ross, J. S.; Wu, S.; Aivazian, G.; Klement, P.; Seyler, K.; Clark, G.; Ghimire, N. J.; Yan, J.; Mandrus, D. G.; Yao, W.; Xu, X. Observation of Long-Lived Interlayer Excitons in Monolayer MoSe_2 – WSe_2 Heterostructures. *Nat. Commun.* **2015**, *6*, 6242.
- (8) Li, L. Y., Yijun Ye, Guo Jun Ge, Qingqin Ou, Xuedong Wu, Hua Feng, Donglai Chen, Xian Hui Zhang, Yuanbo. Black Phosphorus Field-Effect Transistors. *Nat. Nanotechnol.* **2014**, *9*, 372-377.
- (9) Qiao, J.; Kong, X.; Hu, Z.-X.; Yang, F.; Ji, W. High-Mobility Transport Anisotropy and Linear Dichroism in Few-Layer Black Phosphorus. *Nat. Commun.* **2014**, *5*, 4475.
- (10) Xia, F.; Wang, H.; Jia, Y. Rediscovering Black Phosphorus as an Anisotropic Layered Material for Optoelectronics and Electronics. *Nat. Commun.* **2014**, *5*, 4458.

- (11) Low, T.; Rodin, A. S.; Carvalho, A.; Jiang, Y.; Wang, H.; Xia, F.; Castro Neto, A. H. Tunable Optical Properties of Multilayer Black Phosphorus Thin Films. *Phys. Rev. B* **2014**, *90*, 075434.
- (12) Shulenburger, L.; Baczewski, A. D.; Zhu, Z.; Guan, J.; Tománek, D. The Nature of the Interlayer Interaction in Bulk and Few-Layer Phosphorus. *Nano Lett.* **2015**, *15*, 8170-8175.
- (13) Sansone, G.; Maschio, L.; Usvyat, D.; Schütz, M.; Karttunen, A. Toward an Accurate Estimate of the Exfoliation Energy of Black Phosphorus: A Periodic Quantum Chemical Approach. *J. Phys. Chem. Lett.* **2016**, *7*, 131-136.
- (14) Hu, Z.-X.; Kong, X.; Qiao, J.; Normand, B.; Ji, W. Interlayer Electronic Hybridization Leads to Exceptional Thickness-Dependent Vibrational Properties in Few-Layer Black Phosphorus. *Nanoscale* **2016**, *8*, 2740-2750.
- (15) Schütz, M.; Maschio, L.; Karttunen, A. J.; Usvyat, D. Exfoliation Energy of Black Phosphorus Revisited: A Coupled Cluster Benchmark. *J. Phys. Chem. Lett.* **2017**, *8*, 1290-1294.
- (16) Dong, S.; Zhang, A.; Liu, K.; Ji, J.; Ye, Y. G.; Luo, X. G.; Chen, X. H.; Ma, X.; Jie, Y.; Chen, C.; Wang, X.; Zhang, Q. Ultralow-Frequency Collective Compression Mode and Strong Interlayer Coupling in Multilayer Black Phosphorus. *Phys. Rev. Lett.* **2016**, *116*, 087401.
- (17) Ling, X.; Liang, L.; Huang, S.; Piretzky, A. A.; Geohegan, D. B.; Sumpter, B. G.; Kong, J.; Meunier, V.; Dresselhaus, M. S. Low-Frequency Interlayer Breathing Modes in Few-Layer Black Phosphorus. *Nano Lett.* **2015**, *15*, 4080-4088.

- (18) Luo, X.; Lu, X.; Koon, G. K. W.; Castro Neto, A. H.; Özyilmaz, B.; Xiong, Q.; Quek, S. Y. Large Frequency Change with Thickness in Interlayer Breathing Mode—Significant Interlayer Interactions in Few Layer Black Phosphorus. *Nano Lett.* **2015**, *15*, 3931-3938.
- (19) Lui, C. H.; Heinz, T. F. Measurement of Layer Breathing Mode Vibrations in Few-Layer Graphene. *Phys. Rev. B* **2013**, *87*, 121404.
- (20) Lui, C. H.; Malard, L. M.; Kim, S.; Lantz, G.; Laverge, F. E.; Saito, R.; Heinz, T. F. Observation of Layer-Breathing Mode Vibrations in Few-Layer Graphene through Combination Raman Scattering. *Nano Lett.* **2012**, *12*, 5539-5544.
- (21) Tan, P. H.; Han, W. P.; Zhao, W. J.; Wu, Z. H.; Chang, K.; Wang, H.; Wang, Y. F.; Bonini, N.; Marzari, N.; Pugno, N.; Savini, G.; Lombardo, A.; Ferrari, A. C. The Shear Mode of Multilayer Graphene. *Nat. Mater.* **2012**, *11*, 294-300.
- (22) Ni, Z. H.; Wang, H. M.; Kasim, J.; Fan, H. M.; Yu, T.; Wu, Y. H.; Feng, Y. P.; Shen, Z. X. Graphene Thickness Determination Using Reflection and Contrast Spectroscopy. *Nano Lett.* **2007**, *7*, 2758-2763.
- (23) Mao, N.; Wang, X.; Lin, Y.; Sumpter, B. G.; Ji, Q.; Palacios, T.; Huang, S.; Meunier, V.; Dresselhaus, M. S.; Tisdale, W. A.; Liang, L.; Ling, X.; Kong, J. Direct Observation of Symmetry-Dependent Electron–Phonon Coupling in Black Phosphorus. *J. Am. Chem. Soc.* **2019**, *141*, 18994-19001.
- (24) Ling, X.; Huang, S.; Hasdeo, E. H.; Liang, L.; Parkin, W. M.; Tatsumi, Y.; Nugraha, A. R.; Poretzky, A. A.; Das, P. M.; Sumpter, B. G.; Geohegan, D. B.; Kong, J.; Saito,

R.; Drndic, M.; Meunier, V.; Dresselhaus, M. S. Anisotropic Electron-Photon and Electron-Phonon Interactions in Black Phosphorus. *Nano Lett.* **2016**, *16*, 2260-2267.

(25) Wu, J.; Mao, N.; Xie, L.; Xu, H.; Zhang, J. Identifying the Crystalline Orientation of Black Phosphorus Using Angle-Resolved Polarized Raman Spectroscopy. *Angew. Chem. Int. Ed.* **2015**, *54*, 2366-2369.

(26) Cai, Y.; Ke, Q.; Zhang, G.; Feng, Y. P.; Shenoy, V. B.; Zhang, Y.-W. Giant Phononic Anisotropy and Unusual Anharmonicity of Phosphorene: Interlayer Coupling and Strain Engineering. *Adv. Funct. Mater.* **2015**, *25*, 2230-2236.

(27) Zhang, X.; Han, W. P.; Wu, J. B.; Milana, S.; Lu, Y.; Li, Q. Q.; Ferrari, A. C.; Tan, P. H. Raman Spectroscopy of Shear and Layer Breathing Modes in Multilayer MoS_2 . *Phys. Rev. B* **2013**, *87*, 115413.

(28) Froehlicher, G.; Lorchat, E.; Fernique, F.; Joshi, C.; Molina-Sánchez, A.; Wirtz, L.; Berciaud, S. Unified Description of the Optical Phonon Modes in N-Layer MoTe_2 . *Nano Lett.* **2015**, *15*, 6481-6489.

(29) Zhang, G.; Huang, S.; Chaves, A.; Song, C.; Özçelik, V. O.; Low, T.; Yan, H. Infrared Fingerprints of Few-Layer Black Phosphorus. *Nat. Commun.* **2017**, *8*, 14071.

(30) Zhang, G.; Chaves, A.; Huang, S.; Wang, F.; Xing, Q.; Low, T.; Yan, H. Determination of Layer-Dependent Exciton Binding Energies in Few-Layer Black Phosphorus. *Sci. Adv.* **2018**, *4*, eaap9977.

- (31) Liang, L.; Puretzky, A. A.; Sumpter, B. G.; Meunier, V. Interlayer Bond Polarizability Model for Stacking-Dependent Low-Frequency Raman Scattering in Layered Materials. *Nanoscale* **2017**, *9*, 15340-15355.
- (32) Liang, L.; Zhang, J.; Sumpter, B. G.; Tan, Q.-H.; Tan, P.-H.; Meunier, V. Low-Frequency Shear and Layer-Breathing Modes in Raman Scattering of Two-Dimensional Materials. *ACS Nano* **2017**, *11*, 11777-11802.
- (33) Favron, A.; Goudreault, F. A.; Gosselin, V.; Groulx, J.; Côté, M.; Leonelli, R.; Germain, J.-F.; Phaneuf-L'Heureux, A.-L.; Francoeur, S.; Martel, R. Second-Order Raman Scattering in Exfoliated Black Phosphorus. *Nano Lett.* **2018**, *18*, 1018-1027.
- (34) Kim, J.; Lee, J. U.; Lee, J.; Park, H. J.; Lee, Z.; Lee, C.; Cheong, H. Anomalous Polarization Dependence of Raman Scattering and Crystallographic Orientation of Black Phosphorus. *Nanoscale* **2015**, *7*, 18708-18715.
- (35) Phaneuf-L'Heureux, A. L.; Favron, A.; Germain, J. F.; Lavoie, P.; Desjardins, P.; Leonelli, R.; Martel, R.; Francoeur, S. Polarization-Resolved Raman Study of Bulk-Like and Davydov-Induced Vibrational Modes of Exfoliated Black Phosphorus. *Nano Lett.* **2016**, *16*, 7761-7767.
- (36) Ribeiro, H. B.; Pimenta, M. A.; de Matos, C. J. S. Raman Spectroscopy in Black Phosphorus. *J. Raman Spectrosc.* **2018**, *49*, 76-90.
- (37) Mao, N.; Zhang, S.; Wu, J.; Zhang, J.; Tong, L. Lattice Vibration and Raman Scattering in Anisotropic Black Phosphorus Crystals. *Small Methods* **2018**, *0*, 1700409.

- (38) Miao, X.; Zhang, G.; Wang, F.; Yan, H.; Ji, M. Layer-Dependent Ultrafast Carrier and Coherent Phonon Dynamics in Black Phosphorus. *Nano Lett.* **2018**, *18*, 3053-3059.
- (39) Fujii, Y.; Akahama, Y.; Endo, S.; Narita, S.; Yamada, Y.; Shirane, G. Inelastic Neutron Scattering Study of Acoustic Phonons of Black Phosphorus. *Solid State Commun.* **1982**, *44*, 579-582.
- (40) Yamada, Y.; Fujii, Y.; Akahama, Y.; Endo, S.; Narita, S.; Axe, J. D.; McWhan, D. B. Lattice-Dynamical Properties of Black Phosphorus under Pressure Studied by Inelastic Neutron Scattering. *Phys. Rev. B* **1984**, *30*, 2410-2413.
- (41) Lui, C. H.; Ye, Z.; Keiser, C.; Xiao, X.; He, R. Temperature-Activated Layer-Breathing Vibrations in Few-Layer Graphene. *Nano Lett.* **2014**, *14*, 4615-4621.

TOC

